Journal of Thermal Analysis and Calorimetry (2019) 137:811–823
https://doi.org/10.1007/s10973-019-08010-4

Thermal conversion of tobacco stem into gaseous products

Chunhao Wang[1] · Liqing Li[1] · Ruofei Chen[1] · Xiancheng Ma[1] · Mingming Lu[2] · Weiwu Ma[1] · Haoyi Peng[1]

Received: 4 January 2018 / Accepted: 7 January 2019 / Published online: 16 January 2019

Abstract

The pyrolysis of tobacco stem (TS), a potential source of lignocellulosic biomass, is investigated, focusing on gas formation via thermogravimetric analysis–mass spectrometry to obtain accurate gaseous product distributions under various conditions. The results revealed that the majority of the gaseous products were formed under 900 K with a shoulder pyrolysis region (600–800 K) as the main source of gas formation, where the formation curve of CO_2 was used to track the pyrolysis of hemicellulose, cellulose, and lignin. The formation of four aromatics from lignin occurred over the range of 500–900 K, roughly in the sequence of phenol, toluene, xylene, and benzene. Furthermore, the demineralization of TS with HCl did not lead to optimal results, with increased phenol and decreased syngas production, whereas pretreatment with NaOH for hydrolysis was found to significantly increase methane production and decrease the amount of aromatics formed, suggesting that this method should lead to superior results and a simpler reaction mechanism.

Keywords Tobacco stem · Chemical pretreatment · Thermal conversion · TG-MS · Gaseous product distributions · Kinetics of pyrolysis

Introduction

Tobacco stem (TS) is the discarded waste from cigarette manufacturing, accounting for over 20% of the mass of flue-cured tobacco leaves, and must be separated from the usable lamina during cigarette processing. China's tobacco industry has experienced a major transformation since 2003, with an increase in production from 1.8 trillion cigarettes in 2003 to 2.5 trillion cigarettes in 2012 [1]. According to data from the National Bureau of Statistics of China, tobacco leaf yields were 2.8 million tons in 2015 with a cultivation area of approximately 1.3 million hectares. Hence, issues such as pollution prevention and waste management are of key importance to prevent soil and water contamination from landfill sites [2], as nicotine, a toxic and water-soluble substance, is hard to contain once leaching has occurred.

Numerous studies have investigated alternative management strategies for tobacco stem wastes. The proposed applications include the recovery of nicotine [3] and chlorogenic acid [4], and the production of reconstituted tobacco sheet [5, 6], insecticides [7], biosorption materials [8], adsorbents [9], composts [10, 11], and methane [12]. Energy is increasingly becoming an issue of worldwide concern, and pyrolysis technologies for transforming biomass into fuels (syngas, bio-oil, and char) will become more and more important. Polat et al. [13, 14] have investigated the volatile products and mechanism of TS pyrolysis, but the results were hard to interpret and bore no obvious relationship to the stem ingredients. Although many thermal studies have focused on the applications of biomass-derived oil [15–18] and char/carbon [19, 20], the gaseous products have received comparatively little attention [18]. Gas production requires a slow heating rate, high final temperature, and a long gas residence time [21], and the thermal decomposition predominantly involves three major components, cellulose, hemicellulose, and lignin [22], making extraction pretreatment vital. Alkaline

Electronic supplementary material The online version of this article (https://doi.org/10.1007/s10973-019-08010-4) contains supplementary material, which is available to authorized users.

✉ Liqing Li
liqingli@hotmail.com

[1] School of Energy Science and Engineering, Central South University, Changsha 410083, China

[2] School of Energy, Environment, Biological and Medical Engineering, University of Cincinnati, Cincinnati, OH, USA

hydrolysis pretreatment is typically used to digest the biomass components, especially for cellulose and lignin solubilization [23]. Acidic hydrolysis pretreatment has also been used to remove alkali and alkaline-earth metals to avoid catalytic reactions [24, 25]. Furthermore, kinetic modeling of the differential thermogravimetric (DTG) data using three pseudo-components was reported to provide a deeper insight into the pyrolysis process [26–28], particularly the apparent activation energy (AAE).

In this study, the thermogravimetric analysis–mass spectrometry (TG-MS)-based pyrolysis of TS and pretreated samples was investigated, in an attempt to obtain detailed information regarding the structure, composition, thermal behavior, gaseous products, and kinetic mechanism. Several TS samples were studied under different experimental conditions involving different heat/mass transfer considerations, and the correlations between eight kinds of evolved substances and the pyrolysis of three major plant components were investigated, to give a more accurate insight into the pyrolysis of TS, assuming that no interactions exist between each component and the volatile substances.

Materials and methods

Materials and extraction methods

The tobacco stem used in this work was collected from Chenzhou Cigarette Factory, Hunan Province, China. Samples of raw tobacco stem (R-TS) were treated with water, HCl, or NaOH solution, to afford the samples referred to here as W-TS, H-TS, and OH-TS, respectively. The extractions were performed by soaking approximately 50 g of the as-received R-TS in 500 mL of distilled water or NaOH or HCl solutions (0.5 mol L^{-1}) for 2 days. Note that the extraction solutions were replaced with fresh solutions every 8 h. All three extractions were performed at room temperature. The residual liquids were then discarded and the samples were washed with distilled water and placed into a drying oven at 60 °C for 24 h. After crushing and sieving, the powdered feedstock (60 mesh) of W-TS, H-TS, and OH-TS were obtained.

Chemical and structural analysis

The proximate analysis of ash (ASH), volatile matter (VM), and moisture (M) was performed according to the ASTM standard test methods E1755-01, E872-82, and E871-82, respectively, from which the content of fixed carbon (FC) can be calculated by the difference. The ash obtained for each sample was further analyzed regarding the inorganic element content by inductively coupled plasma optical emission spectroscopy (ICP-OES, SPECTROBLUE SOP, Spectro, Germany). The organic elemental analysis was performed using an EA3000 instrument (EuroVector, Italy) and the contents of cellulose, hemicellulose, and lignin were determined via van Soest's method coupled with the Fibretherm FT 12 apparatus (C. Gerhardt, Germany). The Fourier-transform infrared (FT-IR) spectra were measured using an FT-IR spectrometer (Nicolet 6700, Thermo Scientific) for functional groups analysis.

Pyrolysis experiments and product analysis

Both thermogravimetric analysis (TGA) and differential scanning calorimetry (DSC) were conducted using an SDT Q600 instrument (TA Instruments). Moreover, TG-MS was applied for gas detection. Note that for the DSC and kinetic model, samples of approximately 3 mg were pyrolyzed, while 20 ± 0.5 mg samples were pyrolyzed for the TG-MS analysis. Experiments were conducted under high-purity argon gas (20 mL min^{-1}) using different heating rates (10, 20, 40 K min^{-1}) up to ca. 1100 K. The transfer capillary tube of MS was connected to the outlet port of TG, and was heated to 200 °C. The gases were scanned from 1 to 200 amu at a rate of 5 amu s^{-1} by MS. Note that the obtained results regarding different heating rates are referred to as TS-10, TS-20, and TS-40.

Non-isothermal model-free methods

Considering that pyrolysis is a heterogeneous reaction (conversion from solid to volatile gaseous matter), kinetic models typically employ solid-phase conversion [26] and Arrhenius theory [29] to describe the extent of reaction. Normally, the computational work is based on the thermogravimetric data to obtain the apparent kinetic triplets, i.e., the activation energy E, pre-exponential factor A, and kinetic equation $f(\alpha)$. The core principle of the model-free method is that the conversion rate $d\alpha/dt$ is only a function of temperature, without the prior assumption of kinetic equation, as described in Eq. (1) [26]. The Friedman method [30] (Eq. 2) has been widely used to calculate the apparent activation energy E by linear regression. In most cases, E is a function of α, which can be obtained by a least-squares fitting method.

$$\left[\frac{\mathrm{d}\ln(\mathrm{d}\alpha/\mathrm{d}t)}{\mathrm{d}(1/T)}\right]_{\alpha} = -\frac{E_{\alpha}}{R} \tag{1}$$

$$\ln\left(\beta\frac{\mathrm{d}\alpha}{\mathrm{d}T}\right) = \ln[Af(\alpha)] - \frac{E}{\mathrm{R}}\cdot\frac{1}{T} \tag{2}$$

Results and discussion

Characterization of tobacco stem

The compositions of the TS samples before and after the extractions are listed in Table 1. The HCl pretreatment increased the higher heating value (HHV), while the highest carbon-to-hydrogen (C/H) ratio, which influences the effective heating value, was observed for the R-TS sample. Also, HCl pretreatment had the strongest demineralization effect according to the inorganic elemental analysis, especially for K, Mg, and Ca, whereas NaOH led to impregnation with Na and resulted in a very high ash content. The proximate analysis revealed a relatively high content of volatile matter (over 60%), indicating the good performance of gas formation, especially when ash was significantly removed. Furthermore, the HCl pretreatment was found to substantially reduce the level of hemicellulose, whereas the NaOH pretreatment had a similar effect on the level of cellulose.

The FT-IR spectra of the four TS samples are presented in Fig. 1. TS mainly consists of cellulose, hemicellulose, and lignin, alongside smaller amounts of pectin, protein, and water-soluble material [31]. Note that low molecular mass gases typically arise from the cracking and reforming of chemical groups.

The assignment of the spectral bands was based on the literature data [32–34]. The broad and intense absorption peak at 3000–3600 cm^{-1} corresponds to H-bonded O–H and N–H groups [35], which can be ascribed to cellulose, hemicellulose, lignin, pectin, and absorbed water. The bands in the region between 2843 and 3000 cm^{-1} are due to aliphatic C–H stretching, which are most likely attributable to the methylene (–CH_2–) bonds. The two partially overlapping peaks at around 1740 and 1621 cm^{-1} were assigned to the C=O stretching modes of ester and

Table 1 Elemental analysis, proximate analysis, and structural analysis of tobacco stem and treated samples

	R-TS	W-TS	H-TS	OH-TS
Organic elemental analysis/mass%				
C	36.222	38.911	42.806	36.262
H	5.109	5.934	6.130	5.361
N	1.890	1.334	1.273	1.006
S	0.586	0.767	0.615	0.663
O[a]	34.423	43.214	48.796	36.658
C/H	7.090	6.557	6.983	6.764
HHV/MJ kg^{-1}[b]	14.6767	15.9569	17.1556	14.8139
Inorganic elemental analysis				
Na/ppm	43.54	186.96	154.28	49,523.50
K/ppm	70,317.10	915.12	43.70	401.00
Mg/ppm	3635.59	2095.92	19.00	2025.05
Ca/%	3.14	3.70	0.114	3.19
Al/ppm	82.73	51.17	22.04	78.20
Fe/ppm	54.43	68.88	98.80	68.17
Cu/ppm	10.67	9.15	2.96	6.82
Zn/ppm	37.01	26.57	3.00	28.07
Si/ppm	119.74	98.40	39.90	76.19
Proximate analysis/mass%				
M	5.89	4.67	4.03	4.05
VM	61.65	70.52	70.57	67.15
FC[a]	10.69	14.97	25.02	8.75
ASH	21.77	9.84	0.38	20.05
Structural analysis (dry ash-free basis/mass%)				
Cellulose	60.0	50.9	58.1	38.7
Hemicellulose	19.4	19.6	14.9	19.3
Lignin	20.6	29.4	27.0	42.0

[a]Calculated by difference: O/% = 100 − (C + H + N + S + ASH), FC/% = 100 − M − VM − ASH

[b]The higher heating value (HHV) was obtained from the formula established by Channiwala and Parikh [47]: HHV = 0.3491C + 1.1783H + 0.1005S − 0.1034O − 0.0151N − 0.0211ASH/MJ kg^{-1}

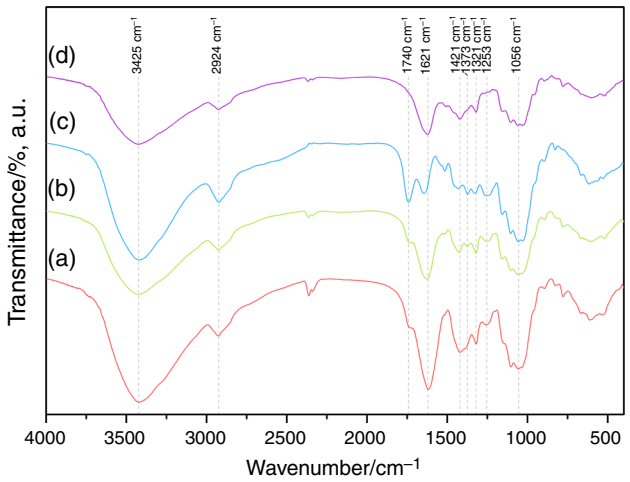

Fig. 1 FT-IR spectra of (*a*) R-TS, (*b*) W-TS, (*c*) H-TS, and (*d*) OH-TS

acid moieties and the aromatic skeletal C=C vibrations in lignin, respectively. The peak at 1421 cm^{-1} could be due to aliphatic and aromatic C–H groups in the plane deformation vibrations of methyl, methylene, and methoxy groups [36]. The peaks at around 1373 and 1321 cm^{-1} were assigned to the O–H/C–H and C–O stretching vibrations, respectively. A strong band was also observed at 1056 cm^{-1}, which could be ascribed to the stretching vibrations of the C–O and C–O–C groups. Bands corresponding to skeletal vibrations often occur at lower wavenumbers, but these are difficult to interpret.

Upon comparing the spectra of the four samples, the intensities of the ester band at 1740 cm^{-1} and the phenolic ether band at 1253 cm^{-1} were found to considerably weaken after the NaOH pretreatment, which has also been reported in the literature for the treatment of rice straw with KOH and indicates that the ester and ether bonds of the lignin in the cross-linking structure can be damaged by hydroxide [34]. Similarly, the HCl pretreatment led to a significant decrease in the band intensity at around 1621 cm^{-1}, which is generally considered to be a lignin marker since among the three major plant polymers only lignin consists of abundant aromatic rings.

Figure 2 shows the SEM images of the raw and pretreated samples, both the surface and interior of each sample were compared. Many small particles are found to be adhered to the surface of the raw TS sample shown in Fig. 2a. A more compact and close-linked fiber structure can be seen in Fig. 2c for the sample pretreated with distilled water, which had washed away most of the small particles. As shown in Fig. 2e, the HCl pretreatment was found to lead to the erosion of some parts of the structure, which became fuzzy but were not completely destroyed. These fuzzy parts are much more abundant for the NaOH-pretreated sample shown in Fig. 2g, indicating more severe corrosion of the sample under these conditions. In the interior images of the TS samples shown in Fig. 2b, d, f, h, the structure of the xylem can be clearly seen [37]. The interior image of the raw sample also revealed many attachments that were very different from the surface image, which may arise from both the particles and the cross-linking structure. However, these were removed by the water and HCl pretreatments, especially the latter, and the undamaged skeleton can be more clearly observed. It therefore appears that the HCl pretreatment did not cause breakage of the skeleton, while it did partially remove the cross-linking structures such as hemicellulose and lignin, which was also demonstrated by the structural analysis results discussed above. The interior of the NaOH-pretreated TS sample appeared to be a disordered array of undetermined material, but the compositional analysis results indicate that this was likely a mixture of dissociated organic tissues and inorganic hydroxides.

Thermal decomposition behavior of tobacco stem

The typical thermal decomposition behavior of the raw TS sample is presented in Fig. 3a. Approximately five peaks (as marked) were observed in the DTG curve according to temperature. Peak 1 at approximately 373 K originated from the moisture retained in the samples. The mass loss in the temperature range of approximately 400–450 K may result from both the decomposition of tobacco components and the vaporization of non-polymeric tobacco constituents [31, 38]. The following two strong and clearly distinguishable peaks, peaks 3 and 4, correspond to hemicellulose and cellulose, respectively. Peak 5 at approximately 1000 K was ascribed to the dehydrogenation and aromatization of char as well as the decomposition of endogenous inorganic compounds such as carbonates. However, lignin is known to decompose slowly over a broad temperature range, and this process was considered to be responsible for the shoulder in the DTG curve located to the right of peak 4 between 600 and 800 K [38, 39]. Each sample was pyrolyzed at heating rates of 10 and 40 K min^{-1}. It can be seen that the curves were displaced to higher temperatures at the faster heating rate, as would be predicted from kinetic theory.

Tobacco stem contains significant amounts of non-structural constituents such as nicotine [3] and chlorogenic acid [4], which could affect the thermal decomposition behavior of cell wall polymers and lead to distinct decomposition patterns. The decomposition patterns of the samples pretreated with water, HCl, or NaOH are shown in Fig. 3b–d, respectively.

Compared with the raw TS sample, five peaks were also observed for the pretreated samples except in the case of

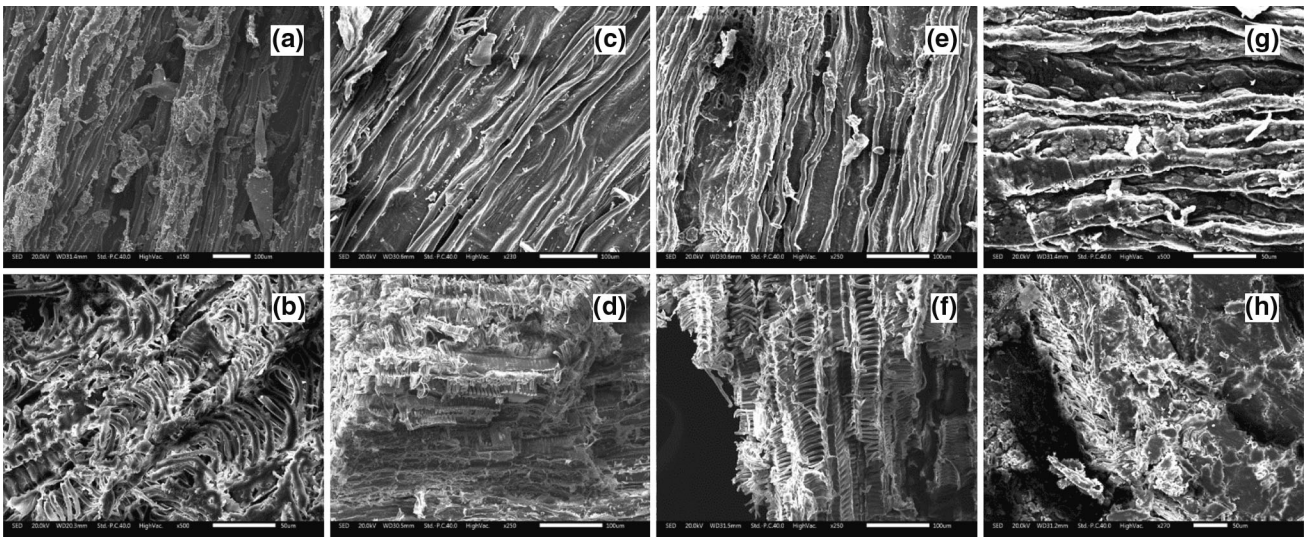

Fig. 2 SEM images of the (**a**, **c**, **e**, **g**) surface and (**b**, **d**, **f**, **h**) interior structures of **a**, **b** R-TS, **c**, **d** W-TS, **e**, **f** H-TS, and **g**, **h** OH-TS

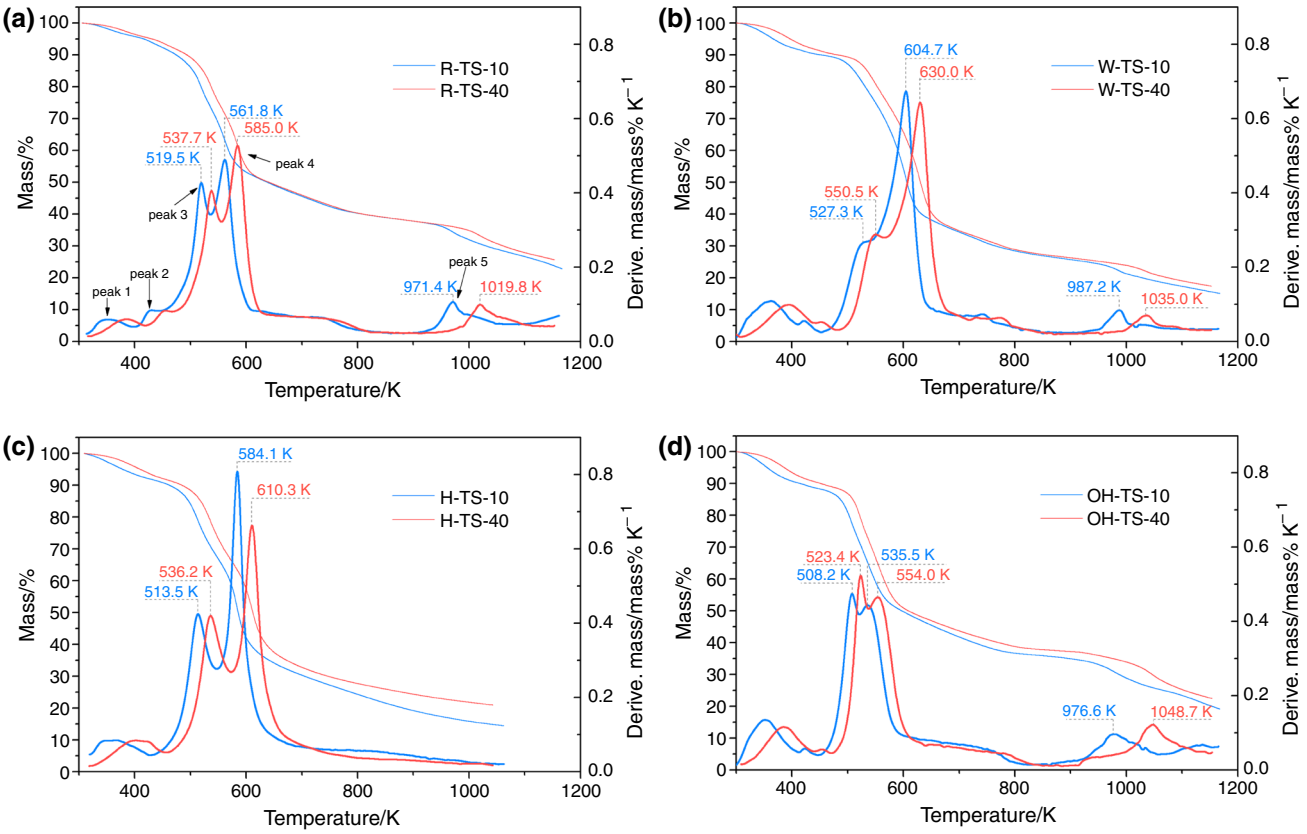

Fig. 3 TG and DTG curves of **a** R-TS, **b** W-TS, **c** H-TS, and **d** OH-TS

H-TS (Fig. 3c). In the latter case, two of the DTG peaks (peaks 2 and 5) as well as the lignin shoulder were significantly reduced. The FT-IR and structural analysis results indicate that the lignin was not entirely removed, the HCl pretreatment therefore led to the removal of a large portion of the non-polymeric constituents and lignin. After the water and HCl treatments, all of the peaks shifted to higher temperatures [33]. This phenomenon can be ascribed to the decrease in catalytic reactions mainly caused by inorganic species [40], as demonstrated in Table 1 by the massive reduction in the contents of inorganic elements in the W-TS and H-TS samples. Therefore, demineralization

will increase the maximum rate of mass loss of cellulose and shift the peaks to higher temperatures, but does not significantly affect the other two peaks [41], which can be verified from the higher gap between the peak temperatures of hemicellulose and cellulose. The NaOH pretreatment led to the opposite effect given the vast impregnation of the sample with Na^+ ions, which illustrates that the metallic ion Na^+ may cause catalysis and lower the reaction temperature.

As for the reaction intensity, the intensity of peak 3 remained almost steady with a value of ca. 0.4 mass% K^{-1}, except in the case of W-TS, which was reduced to ca. 0.3 mass% K^{-1}. The intensity changes of peak 4 in the W-TS and H-TS samples showed the same trend as these samples contain less inorganic material resulting in a higher reaction rate, while the R-TS and OH-TS samples gave the opposite results. These results may indicate the strong dependence of cellulose pyrolysis on the existence of sufficient inorganic species, which will typically reduce the reaction intensity, but the precise nature of the species responsible remains unclear [42]. In terms of peak 5, which we considered to represent lignin pyrolysis, little change was observed.

Gaseous product distributions

Prior to the analysis of the mass spectrometric data, we carefully compared the base peaks (or molecular ion peaks) and fragment ion peaks of each of the possible components (the charge states are described in Table 2), and finally obtained the following identifications: mass-to-charge ratios (m/z) of 15, 17, 30, 44, 78, 92, 94, and 106 corresponded to methane (CH_4), water vapor (H_2O), carbon monoxide (CO), carbon dioxide (CO_2), benzene (C_6H_6), toluene (C_7H_8), phenol (C_6H_6O), and xylene (C_8H_{10}), respectively. It should be noted that temperature shifting occurred because of the delay of several seconds required for gas transportation between the crucible and the detector. 3D waterfall plots of typical MS signal intensity excluding the purge gas (mainly argon with small amounts of nitrogen and oxygen) are shown in Fig. S1. The low m/z region contains multiple low molecular mass gases and was difficult to separate in the 3D waterfall plot, while the high m/z region permits more definitive identification of the various high molecular mass hydrocarbons. In general, acid pretreatment results in a massive increase in the production of high molecular mass hydrocarbons, usually as oil. For all of the TS samples, the precision of the results depended on the heating rate applied; in Figs. 4 and 5, the results for low molecular mass gases and the aromatic species are shown for the heating rates of 10 and 40 K min^{-1}, respectively.

Non-condensible gaseous products

Figure 4 shows the change in detected ion current for non-condensible species versus the calibrated temperature, and the connection between TG and MS will now be discussed. It is feasible from the variation information to discuss at what point both the formation of gases and the pyrolysis of the constituents will occur.

For all four samples, the ion current peak corresponding to CO_2 (Fig. 4d) was found to exhibit a high degree of similarity to the peaks in the DTG curves. It was therefore deduced that the formation of CO_2 accompanies the pyrolysis reactions of all of the main structural carbohydrates throughout the whole temperature range, and CO_2 was therefore taken as the marker gas. Previous studies [43] have also provided FT-IR validation that the three main structural carbohydrates generally underwent pyrolysis to produce more than one gas peak, among which the highest one exactly corresponded to each typical DTG peak. Therefore, the peaks at 541.3, 582.4, and 980.5 K represent the pyrolysis of hemicellulose, cellulose, and

Table 2 The charge states of gas species analyzed, and these data are directly exported from the spectra library in MS software except phenol

Gas species	m/z (relative intensity)
Methane	16 (0.9999); 15 (0.858); 14 (0.156); 13 (0.077); 12 (0.024); 17 (0.012)
Water vapor	18 (0.9999); 17 (0.23); 16 (0.011); 20 (0.003); 19 (0.001)
Carbon dioxide	44 (0.9999); 28 (0.114); 16 (0.085); 12 (0.06); 45 (0.013); 22 (0.012) 46 (0.004); 13 (0.001); 29 (0.001)
Carbon monoxide	28 (0.9999); 12 (0.045); 29 (0.011); 16 (0.009); 14 (0.006); 30 (0.002)
Benzene	78 (0.9999); 52 (0.194); 51 (0.186); 50 (0.157); 77 (0.144); 39 (0.142) 79 (0.0644); 76 (0.06); 38 (0.058)
Toluene	91 (0.9999); 92 (0.785); 50 (0.71); 39 (0.206); 65 (0.138); 51 (0.107) 63 (0.101); 90 (0.091); 27 (0.06); 38 (0.057); 93 (0.055)
Phenol	Using monoisotopic mass ca. 94
Xylene	91 (0.9999); 106 (0.577); 105 (0.241); 39 (0.174); 51 (0.161) 77 (0.127); 27 (0.11); 78 (0.084); 92 (0.075); 107 (0.048)

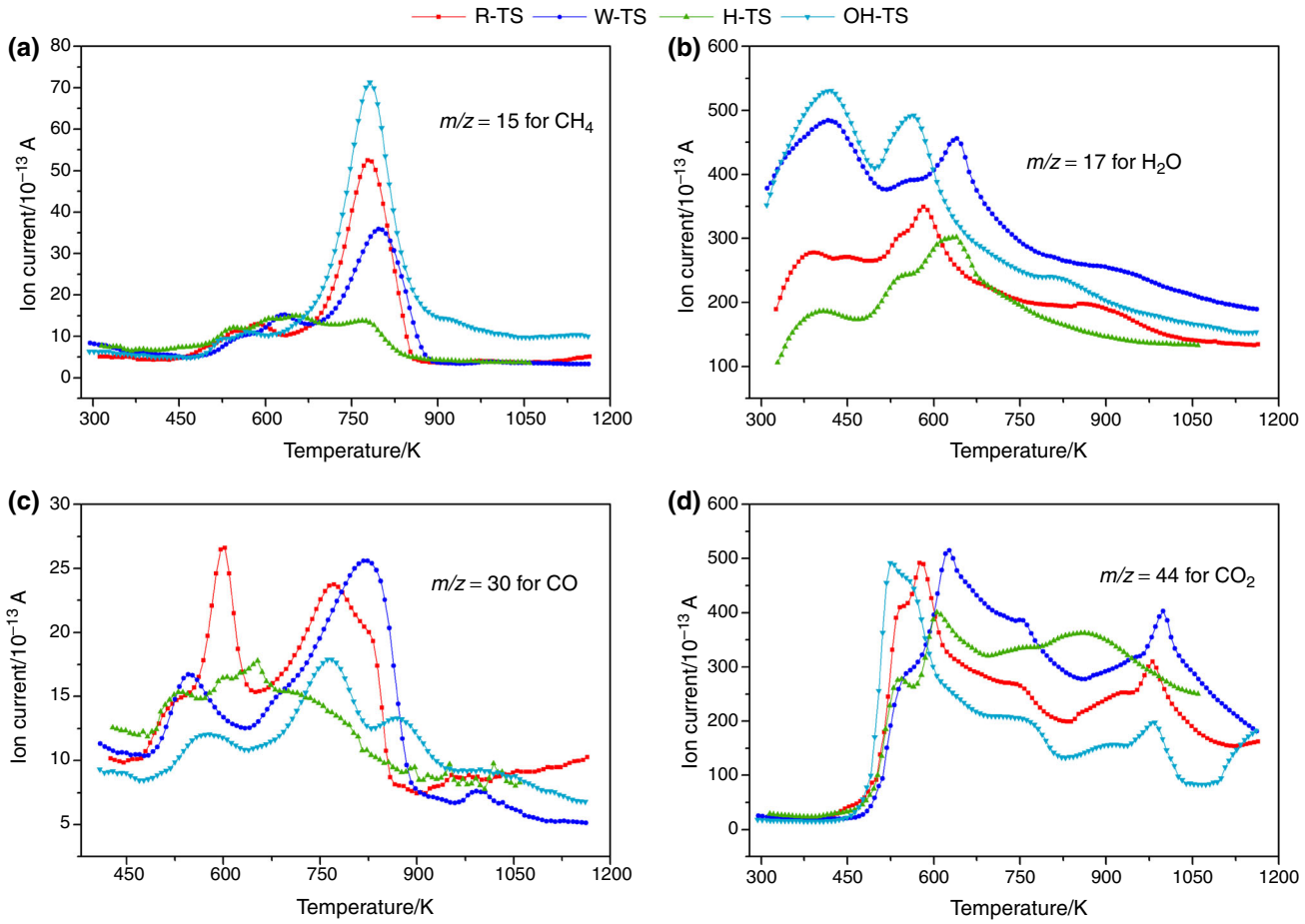

Fig. 4 Analysis of ion current changes detected by MS toward main non-condensible gases: **a** m/z = 15 for CH_4, **b** m/z = 17 for H_2O, **c** m/z = 30 for CO, and **d** m/z = 44 for CO_2

other carbonates (the same shoulder for lignin pyrolysis around 700 K was also observed), respectively, to yield CO_2, which is mainly formed by decarboxylation reactions [43–45]. To confirm this result, the correlation between the peak temperatures for the CO_2 formation curves and DTG curves is presented in Fig. 6, yielding a clear and well-matched linear result. This will be applied to the following analyses with the precondition of no significant interactions occurring among the pyrolysis products. However, a very obvious reduction in CO_2 production from the OH-TS sample was observed for the high-temperature region, indicating that alkali pretreatment may lead to a higher quality of pyrolysis gas. With respect to H_2O in Fig. 4b, three peaks were generally observed, representing loosely bonded water and water formed from dehydroxylation reactions in hemicellulose and cellulose pyrolysis [44].

Although pyrolysis gas consists of a mixture of species, the levels of combustible gases are the main concern. Regarding the production of CH_4 and CO (Fig. 4a, c) from the R-TS sample, peaks corresponding to hemicellulose and cellulose pyrolysis were observed, but in the high-temperature region only CO showed a tendency to increase, which most likely resulted from secondary reactions of both hemicellulose and lignin [43]. It should be noted that both CO and CH_4 showed very strong formation peaks in the shoulder lignin pyrolysis-related region mentioned above for the TG results, and these gases are responsible for the majority of gas production, yet no intense mass loss occurred. It remains unclear whether the CO and CH_4 come from the same source in this region, although this superficially appears to be a lignin-related pyrolysis region. However, Yang et al. [43] have suggested that CO is only derived from hemicellulose while CH_4 comes from both hemicellulose and lignin, and lignin is responsible for most of the CH_4 because of its high methoxy group (–O–CH_3) content and abundant aliphatic side branches [45]. However, this depends on the biomass itself, as it is well known that the composition of hemicellulose and lignin can differ between different sources.

In terms of the comparison of the various samples, differences were observed for the three combustible gases. The intense CO formation peak that appeared for the R-TS

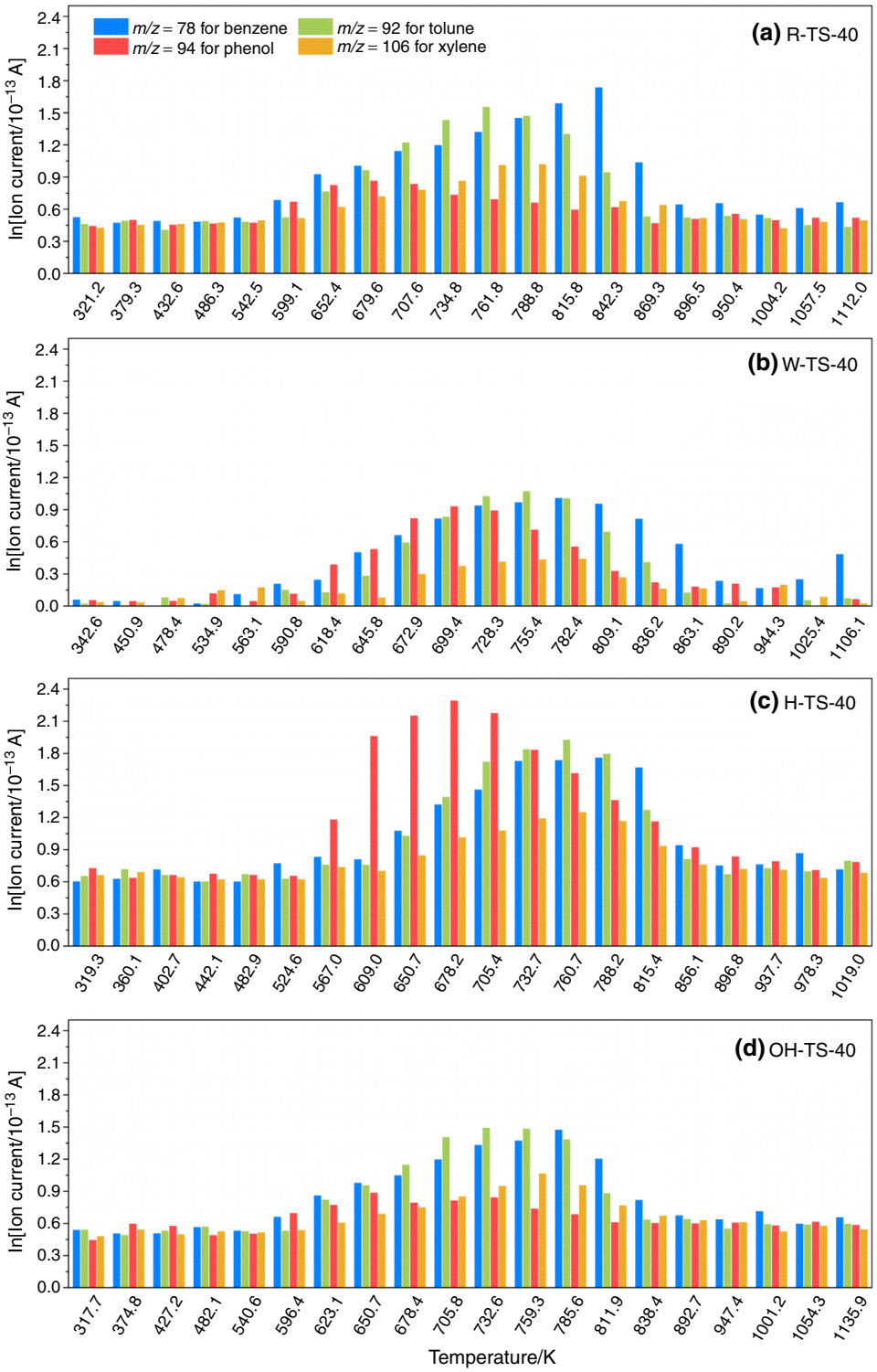

Fig. 5 Analysis of ion current changes detected by MS toward main condensible gases: **a** R-TS-40, **b** W-TS-40, **c** H-TS-40, **d** OH-TS-40

sample at the temperature corresponding to cellulose pyrolysis was either not present or visibly reduced for the other three samples. Cellulose pyrolysis only generates small amounts of CO [43], and thus it should be further confirmed whether this peak is from cellulose or happens only in the presence of certain catalysts. And there was a significant reduction in CO and CH_4 production for H-TS. Significant reduction or structural modification of lignin according to the previous characterization would be expected to cause decreased CH_4 production, while from the decrease in CO production it can be concluded that some of the functional groups in hemicellulose were also

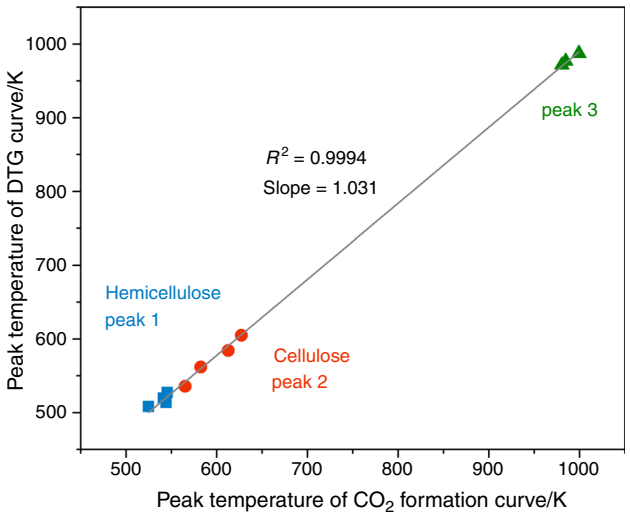

Fig. 6 Correlations between the peak temperatures of the CO_2 formation curve and the DTG curve. All of the data were obtained using the heating rate of 10 K min^{-1}

removed by the acid treatment, such as ether (C–O–C) and carbonyl (C=O) groups, leading to an unexpectedly low gas yield. The same decrease in CO production were also detected for the OH-TS sample, and the residual levels of Na^+ seemed to not have a very strong catalytic effect on cellulose pyrolysis to produce CO. However, a much stronger CH_4 formation peak was clearly observed, and the reason for this is unknown. At higher temperatures, almost no useful gaseous products were observed, so in future investigations it would be recommended to use pyrolysis temperatures of under 900 K.

Condensible gaseous products

Figure 5 also shows the variation of four different aromatic species, because these are important ingredients of oil products that should be condensed in downstream equipment, and Fig. S1 provides a deeper insight into the levels of these species observed in the 3D waterfall plot. Each of the four products exhibited distinct profiles, with the approximate formation sequence of phenol, toluene, xylene, and benzene (PTXB), across a broad temperature range of 500–900 K. As these species are all aromatic hydrocarbons and lignin is the major contributor of aromatic rings and undergoes pyrolysis across a broad temperature range, it can be concluded that lignin decomposition is responsible for the formation of these products. In particular, H-TS yielded the greatest amounts of PTXB, which indicates that the acid pretreatment influenced the original structure, especially in the case of phenol, which is believed to originate from the dissociation of ester-linked lignin fragments in hemicellulose [44]. However, the results of OH-TS and R-TS were very similar with lower yields. Chemically, we can deduce from the above results that the structure of tobacco stem contains a large amount of non-phenolic α-aryl ether bonds, which underwent hydrolysis during the HCl pretreatment to form more phenolic hydroxyl groups, which would not be expected to occur during the NaOH pretreatment. This would also explain the decrease in nearly half of the aromatic skeletal C=C bond vibrations in the FT-IR spectrum of the H-TS sample, which can be understood according to the results of Wu et al. [46] and the mechanism shown in Fig. 7. Moreover, it seems that the presence of inorganic substances had a negative effect on tar formation. However, the yields of benzene and toluene remained high regardless of the conditions, and the yield of xylene was always steady and low. However, the significant mass losses of cellulose and hemicellulose in the TG results can only be accounted for by the formation of other high molecular mass substances, thus making the two components unsuitable for pyrolysis to gaseous products. In conclusion, acid pretreatment seems insufficient because of its increased tar yield and reduced syngas production.

Pyrolysis pattern of 3 mg samples of tobacco stem

From the previous pyrolysis results using the 20 mg samples, we determined the existence of two potential problems. The first issue is the influence of the sample quantity on kinetic calculations. It should be taken into consideration that mass and heat transfer will have a huge impact on the results, leading to inaccurate pyrolysis kinetics. Therefore, a small amount of sample (approximately 3 mg) that is plainly and evenly spread in the alumina crucible was found to be sufficient. The second problem is that it is very difficult to define the exact temperature border of lignin pyrolysis as the DTG regions corresponding to cellulose and hemicellulose are irregular and hard to identify. As such, lignin may not be suitable to use for the kinetic calculations involving tobacco stem.

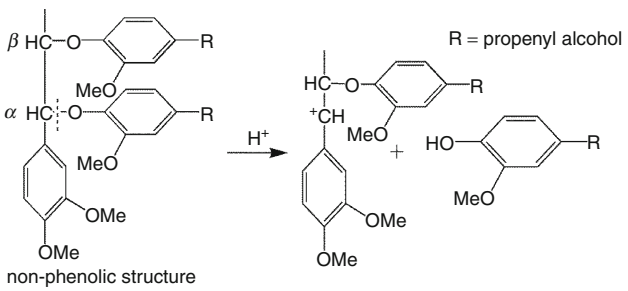

Fig. 7 Acidic hydrolysis of α-aryl ether bonds in non-phenolic structures, where hydrolysis of the β-aryl ether bonds is 100 times slower

In the next set of experiments, the four samples were investigated at three heating rates (10, 20, 40 K min^{-1}). The conversion rate $d\alpha/dT$ and its peak-fitting data as a function of temperature, the DSC signal, and the apparent activation energy E as a function of conversion extent α are shown in Fig. 8 for the R-TS, W-TS, H-TS, and OH-TS samples, where α is deduced from the peak-fitting data. The patterns of the DTG peaks were almost the same as the previous DTG curves using the 20 mg samples, indicating a good reproducibility. The DSC profiles typically exhibited more than one endothermic peak or even an irregular endothermic region, which give general heat change information, and the shoulder region represents the main endothermic reaction.

The DSC signals at the different heating rates exhibited intensity differences but the overall trend was similar, which enables the reaction heat change during pyrolysis to be better understood. For the R-TS samples, three distinct

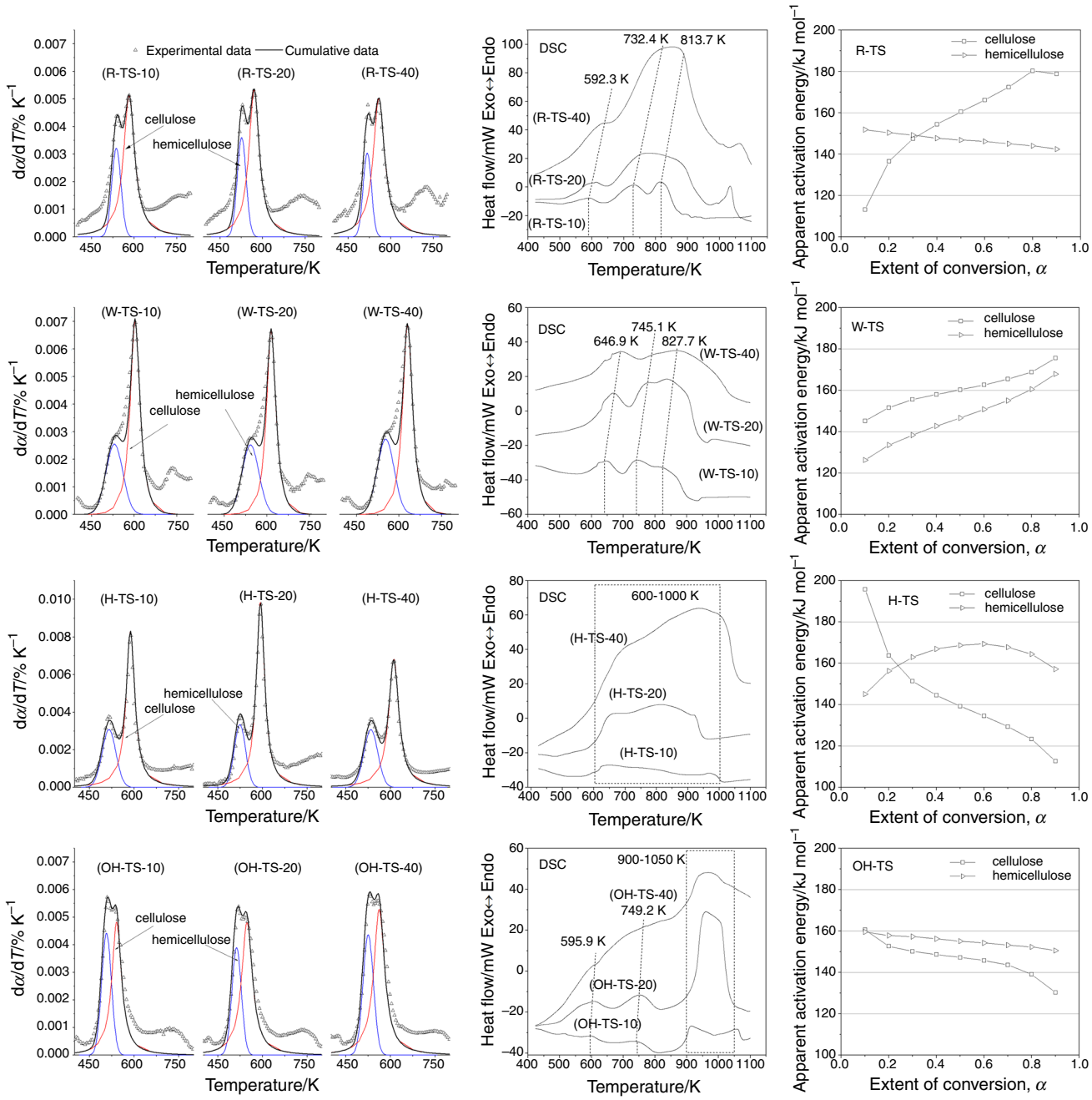

Fig. 8 Pyrolysis using 3 mg of tobacco stem and the treated samples, to obtain accurate results for the conversion rate $d\alpha/dT$ and its peak-fitting data (left), the DSC curve (center), and the apparent activation energy (right) calculated based on the Friedman method

Table 3 Polynomial/linear fitting of apparent activation energy as a function of α and its average values

	Polynomial/linear fitting of $E(\alpha)$/J mol^{-1}[a]	R^2	Average value/J mol^{-1}
R-TS	$E_{c,R} = 92{,}339 + 261{,}260\alpha - 317{,}179\alpha^2 + 151{,}785\alpha^3$	0.987	156,680
	$E_{h,R} = 154{,}646 - 11{,}088\alpha$	0.992	147,102
W-TS	$E_{c,W} = 136{,}384 + 105{,}253\alpha - 171{,}749\alpha^2 + 114{,}558\alpha^3$	0.999	160,399
	$E_{h,W} = 117{,}555 + 100{,}899\alpha - 128{,}963\alpha^2 + 87{,}789\alpha^3$	1	146,918
H-TS	$E_{c,H} = 231{,}354 - 446{,}558\alpha + 729{,}977\alpha^2 - 423{,}960\alpha^3$	0.993	143,843
	$E_{h,H} = 134{,}696 + 125{,}178\alpha - 111{,}070\alpha^2$	0.992	162,113
OH-TS	$E_{c,OH} = 171{,}296 - 134{,}465\alpha + 265{,}437\alpha^2 - 185{,}067\alpha^3$	0.997	146,479
	$E_{h,OH} = 160{,}389 - 10{,}453\alpha$	0.992	155,163

[a] $E_{c,R}$: the apparent activation energy of cellulose of R-TS, for example

endothermic peaks centered at 592.3, 732.4, and 813.7 K were observed. Many investigations have led to the same conclusion that cellulose pyrolysis is endothermic [41], which in the case of Fig. 8 corresponds to the first peak, while the second and third peaks located in the shoulder region may be related to the formation of volatile substances discussed previously, as the cleavage of chemical bonds is an energy-consuming process. At higher heating rates, the latter two peaks overlapped somewhat. The W-TS sample exhibited a relatively weak DSC signal, but three peaks were also observed. The H-TS sample only displayed an irregular DSC profile with an endothermic range from 600 to 1000 K, which did not, however, correspond to an apparent mass loss as mentioned previously. The first two DSC peaks of OH-TS showed a slight difference from those of R-TS, but in the temperature range of 900–1050 K an intense endothermic region was observed, which matches the temperature for other carbonates pyrolysis indicated as peak 5 in Fig. 3d. This is very different from the other samples, and it seems that pyrolysis in this region is strongly catalyzed by NaOH extraction or the resulting Na^+ impregnation.

The apparent activation energy values for cellulose (E_c) and hemicellulose (E_h) were calculated using the Friedman method based on the peak-fitting data, to deliver an estimate of E as a function of the reaction extent α. The detailed linear fitting results based on Eq. (2) are shown in Fig. S2, allowing the slope of each line to be obtained and the apparent activation energy to be calculated as a polynomial/linear function of α. These values are listed in Table 3 as a reference for further research. Note that only the E_h of H-TS did not increase monotonically with the reacted fraction, with a maximum value at $\alpha \approx 0.6$. Both R-TS and OH-TS gave relatively plain E_h profiles throughout the conversion range, which indicate a simple reaction mechanism. In terms of E_c, the four samples showed different patterns. For R-TS and W-TS, E_c increased monotonically, whereas for H-TS and OH-TS it decreased with reaction extent, demonstrating totally different and complex reaction mechanisms, especially in terms of the kinetic equation $f(\alpha)$. In general, E_h will be increased by water extraction and E_c by HCl extraction, although a detailed discussion of $f(\alpha)$ is beyond the scope of this paper.

Conclusions

In this paper, the pyrolysis of tobacco stem was investigated for both raw samples and pretreated samples with water, HCl, and NaOH, to obtain the gas formation process through TG-MS analysis, which generally showed the majority of gases formed below 900 K. The H-TS sample exhibited the worst results, displaying the highest tar (especially phenol) and lowest syngas production, while the best results were obtained for the OH-TS sample, which gave increased CH_4 and reduced tar formation. The CO_2 formation peak was used to track the pyrolysis of hemicellulose, cellulose, and lignin, and found that the majority of useful products were derived from the shoulder region corresponds to lignin pyrolysis. The formation of aromatic species occurring roughly in the sequence of phenol, toluene, xylene, and benzene, can be substantially inhibited by inorganic elemental species. Kinetically, HCl most reduced the E_c and increased E_h, although the pretreatment with NaOH involves a simpler reaction mechanism. This investigation has provided insight into the fundamental thermal transformation behavior for tobacco stem to potentially expand its application in bioenergy technology.

Acknowledgements This work was supported by the National Key Technology Support Program of China (2015BAL04B02), the National Natural Science Foundation of China (No. 21376274), the Collaborative Innovation Center of Building Energy Conservation and Environmental Control, and the Graduate Self-Exploration and Innovation Program of Central South University (2017zzts168).

References

1. Dan X, Yuankai S, Chen W. Tobacco in China. Lancet. 2014;383:2045–6.

2. Mumba P, Phiri R. Environmental impact assessment of tobacco waste disposal. Int J Environ Res. 2008;2:225–30.
3. de Lucas A, Cañizares P, García MA, Gómez J, Rodríguez JF. Recovery of nicotine from aqueous extracts of tobacco wastes by an H + -form strong-acid ion exchanger. Ind Eng Chem Res. 1998;37:4783–91.
4. Li Z, Huang D, Tang Z, Deng C, Zhang X. Fast determination of chlorogenic acid in tobacco residues using microwave-assisted extraction and capillary zone electrophoresis technique. Talanta. 2010;82:1181–5.
5. Ding M, Wei B, Zhang Z, She S, Huang L, Ge S, Sheng L. Effect of potassium organic and inorganic salts on thermal decomposition of reconstituted tobacco sheet. J Therm Anal Calorim. 2017;129:975–84.
6. Gao W, Chen K. Physical properties and thermal behavior of reconstituted tobacco sheet with precipitated calcium carbonate added in the coating process. Cellulose. 2017;24:2581–90.
7. Prabowo H, Martono E, Witjaksono W. Activity of liquid smoke of tobacco stem waste as an ibsecticide on Spodoptera litura Fabricius larvae. Indones J Plant Protect. 2017;20:22–7.
8. Qi B, Aldrich C. Biosorption of heavy metals from aqueous solutions with tobacco dust. Bioresour Technol. 2008;99:5595–601.
9. Ma XC, Li LQ, Chen RF, Wang CH, Zhou K, Li HL. Porous carbon materials based on biomass for acetone adsorption: effect of surface chemistry and porous structure. Appl Surf Sci. 2018;459:657–64.
10. Zhao GH, Feng YJ, Yu YL, Li ZM. Evaluation of stability and maturity during tobacco industrial solid waste composting. Adv Mater Res. 2014;1010–1012:956–60.
11. Saithep N, Dheeranupatana S, Sumrit P, Jeerat S, Boonchalearmkit S, Wongsanoon J, Jatisatienr C. Composting of tobacco plant waste by manual turning and forced aeration system. Maejo Int J Sci Technol. 2009;3:248–60.
12. Meher K, Panchwagh A, Rangrass S, Gollakota K. Biomethanation of tobacco waste. Environ Pollut. 1995;90:199–202.
13. Polat S, Apaydin-Varol E, Pütün AE. Thermal decomposition behavior of tobacco stem Part I: TGA–FTIR–MS analysis. Energy Source Part A. 2016;38:3065–72.
14. Polat S, Apaydin-Varol E, Pütün AE. Thermal decomposition behavior of tobacco stem Part II: kinetic analysis. Energy Source Part A. 2016;38:3073–80.
15. Czernik S, Bridgwater A. Overview of applications of biomass fast pyrolysis oil. Energy Fuel. 2004;18:590–8.
16. Zhang Q, Chang J, Wang TJ, Xu Y. Review of biomass pyrolysis oil properties and upgrading research. Energy Convers Manag. 2007;48:87–92.
17. Mortensen PM, Grunwaldt JD, Jensen PA, Knudsen KG, Jensen AD. A review of catalytic upgrading of bio-oil to engine fuels. Appl Catal A Gen. 2011;407:1–19.
18. Hossain AK, Davies PA. Pyrolysis liquids and gases as alternative fuels in internal combustion engines: a review. Renew Sustain Energy Rev. 2013;21:165–89.
19. Sohi SP, Krull E, Lopez-Capel E, Bol R. A review of biochar and its use and function in soil. Adv Agron. 2010;105:47–82.
20. Samira B, Nurhidayatullaili MuhdJ. Biomass-derived activated carbon: synthesis, functionalized, and photocatalysis application. In: Tawfik AS, editor. Advanced nanomaterials for water engineering, treatment, and hydraulics. Hershey: IGI Global; 2017. p. 162–99.
21. Basu P. Biomass gasification and pyrolysis: practical design and theory. Cambridge: Academic Press; 2010.
22. Wang K, Kim KH, Brown RC. Catalytic pyrolysis of individual components of lignocellulosic biomass. Green Chem. 2014;16:727–35.
23. Carvalheiro F, Duarte LC, Gírio FM. Hemicellulose biorefineries: a review on biomass pretreatments. J Sci Ind Res India. 2008;67:849–64.
24. Long J, Song H, Jun X, Sheng S, Lun-shi S, Kai X, Yao Y. Release characteristics of alkali and alkaline earth metallic species during biomass pyrolysis and steam gasification process. Bioresour Technol. 2012;116:278–84.
25. Nkemka VN, Li Y, Hao X. Effect of thermal and alkaline pretreatment of giant Miscanthus and Chinese fountaingrass on biogas production. Water Sci Technol. 2015;75:849–56.
26. Wang S, Ru B, Lin H, Dai G, Wang Y, Luo Z. Kinetic study on pyrolysis of biomass components: a critical review. Curr Org Chem. 2016;20:2489–513.
27. Vyazovkin S, Burnham AK, Criado JM, Pérez-Maqueda LA, Popescu C, Sbirrazzuoli N. ICTAC Kinetics Committee recommendations for performing kinetic computations on thermal analysis data. Thermochim Acta. 2011;520:1–19.
28. Cai J, Wu W, Liu R, Huber GW. A distributed activation energy model for the pyrolysis of lignocellulosic biomass. Green Chem. 2013;15:1331–40.
29. Bruzs B. Velocity of thermal decomposition of carbonates. J Phys Chem. 1926;30(5):680–93.
30. Friedman HL. Kinetics of thermal degradation of char-forming plastics from thermogravimetry. Application to a phenolic plastic. J Polym Sci Pol Symp. 1964;6:183–95.
31. Sung YJ, Seo YB. Thermogravimetric study on stem biomass of Nicotiana tabacum. Thermochim Acta. 2009;486:1–4.
32. Strezov V, Popovic E, Filkoski RV, Shah P, Evans T. Assessment of the thermal processing behavior of tobacco waste. Energy Fuel. 2012;26:5930–5.
33. Long J, Song H, Sun LS, Sheng S, Kai X, He LM, Xiang J. Influence of different demineralization treatments on physicochemical structure and thermal degradation of biomass. Bioresour Technol. 2013;146:254–60.
34. Oh GH, Yun CH, Park CR. Role of KOH in the one-stage KOH activation of cellulosic biomass. Bioorg Med Chem Lett. 2003;24:4999–5007.
35. Domínguez A, Menéndez J, Inguanzo M, Pis J. Production of biofuels by high temperature pyrolysis of sewage sludge using conventional and microwave heating. Bioresour Technol. 2006;97:1185–93.
36. Köseoğlu E, Akmil-Başar C. Preparation structural evaluation and adsorptive properties of activated carbon from agricultural waste biomass. Adv Powder Technol. 2015;26:811–8.
37. Zhao D, Dai Y, Feng G, Yang J, Song J, She X. Chemical composition and fiber morphology of tobacco stem, scrap and dust. Tob Sci Technol. 2016;49:36–44.
38. Oja V, Hajaligol MR, Waymack BE. The vaporization of semivolatile compounds during tobacco pyrolysis. J Anal Appl Pyrol. 2006;76:117–23.
39. Kastanaki E, Vamvuka D, Grammelis P, Kakaras E. Thermogravimetric studies of the behavior of lignite–biomass blends during devolatilization. Fuel Process Technol. 2002;77–78:159–66.
40. Nowakowski DJ, Jones JM, Brydson RMD, Ross AB. Potassium catalysis in the pyrolysis behaviour of short rotation willow coppice. Fuel. 2007;86:2389–402.
41. Le Brech Y, Ghislain T, Leclerc S, Bouroukba M, Delmotte L, Brosse N, Snape C, Chaimbault P, Dufour A. Effect of potassium on the mechanisms of biomass pyrolysis studied using complementary analytical techniques. Chemsuschem. 2016;9:863–72.
42. Shimada N, Kawamoto H, Saka S. Different action of alkali/alkaline earth metal chlorides on cellulose pyrolysis. J Anal Appl Pyrol. 2008;81:80–7.

43. Yang H, Yan R, Chen H, Lee DH, Zheng C. Characteristics of hemicellulose, cellulose and lignin pyrolysis. Fuel. 2007;86:1781–8.
44. Wang S, Ru B, Dai G, Sun W, Qiu K, Zhou J. Pyrolysis mechanism study of minimally damaged hemicellulose polymers isolated from agricultural waste straw samples. Bioresour Technol. 2015;190:211–8.
45. Wang S, Ru B, Lin H, Sun W, Luo Z. Pyrolysis behaviors of four lignin polymers isolated from the same pine wood. Bioresour Technol. 2015;182:120–7.
46. Wu M, Xue J, Li Q, Tai D, Li T. Estimation of non-cyclic α-aryl ether units in wood and gramineous lignins. J Cell Sci Technol. 1995;3:32–9.
47. Channiwala SA, Parikh PP. A unified correlation for estimating HHV of solid, liquid and gaseous fuels. Fuel. 2002;81:1051–63.